DEUTSCHES ELEKTRONEN-SYNCHROTRON

DESY 93-158
November 1993

Results from the ZEUS Experiment at HERA

H. Abramowicz

Dept. of Nuclear Physics, Weizmann Institute of Science, Rehovot, Israel

R. Klanner

Deutsches Elektronen-Synchrotron DESY, Hamburg

J. F. Martin

Institute of Particle Physics, University of Toronto, Canada

ISSN 0418-9833

NOTKESTRASSE 85 - 22603 HAMBURG

To be sure that your preprints are promptly included in the
HIGH ENERGY PHYSICS INDEX,
send them to (if possible by air mail):

DESY
Bibliothek
Notkestraße 85
22603 Hamburg
Germany

DESY-IfH
Bibliothek
Platanenallee 6
15738 Zeuthen
Germany

DESY 93-158
November 1993

ISSN 0418-9833

Results from the ZEUS Experiment at HERA*

Halina Abramowicz
Department of Nuclear Physics, Weizmann Institute

Robert Klanner
DESY, Hamburg

John F. Martin
Institute of Particle Physics, University of Toronto

ABSTRACT

This is a short overview of the results obtained by the ZEUS Collaboration with data collected during the first year of HERA running and corresponding to an integrated luminosity of 25 nb^{-1}. Included are the measurement of the total, partial and ρ photoproduction cross sections, a study of high mass diffractive photoproduction, new results from hard photoproduction where a clear signal of a direct photon contribution has been established, the measurement of the proton structure function F_2 and first results on diffractive dissociation of the virtual photon in the deep inelastic electron proton scattering. Limits on leptoquarks and excited electrons are also presented.

*Report based on talks given by H. Abramowicz at the Topical Conference at the 1993 SLAC Summer Institute, R. Klanner at the 1993 EPS Conference at Marseille and by J. F. Martin at the 1993 Lepton–Photon Conference at Cornell.

1 HERA and ZEUS

1.1 Introduction

ZEUS is one of the two large experiments at the electron-proton collider HERA, now in operation at DESY in Hamburg. The physicists collaborating in ZEUS come from 46 institutions in 12 countries.

Over the next decade HERA will provide the particle physics community with a unique experimental facility. The high centre of mass energy (296 GeV) extends the kinematic domain of lepton proton scattering, so far studied at fixed target experiments, to much higher Q^2 ($\sim 5 \cdot 10^4$ GeV^2) and to much lower x ($\sim 10^{-4}$). Sensitive tests of QCD and Electroweak theory, detailed studies of diffractive physics and searches for new physics will be made.

In this report we describe the operation of HERA and ZEUS in the first one and a half years of running and give an overview of the significant physics results obtained so far, based mostly on the analysis of the 1992 data.

1.2 The Status of HERA

HERA is designed to collide 30 GeV electrons with 820 GeV protons. The design luminosity of 1.5×10^{31} $cm^{-2}s^{-1}$ requires currents of 58 mA and 163 mA in the electron and proton beams, respectively. The beams are bunched into 210 bunches with an interbunch spacing of 96 ns.

In 1992, the first year of data taking for the experiments, HERA delivered an integrated luminosity of about 30 nb^{-1}, colliding 820 GeV protons with 26.7 GeV electrons in 9 bunches. In addition, single unpaired 'pilot' bunches of electrons and protons circulated, which permitted a measurement of beam associated backgrounds. The maximum luminosity achieved was about 4×10^{29} $cm^{-2}s^{-1}$.

In 1993 HERA has been running with the same beam energies, but with 84 colliding bunches, 10 proton pilot bunches and 6 electron pilot bunches. Typical currents at injection are 16 mA in the electron beam and 14 mA in the proton beam. The proton beam lifetime is longer than 100 hours. Usually one proton fill can be used for several electron fills before the emittance has grown sufficiently to require a new proton fill. The electron beam lifetime in good conditions is 7–10 hours.

The maximum luminosity reached so far by HERA is about 1.6×10^{30} $cm^{-2}s^{-1}$.

The specific luminosity (referring to single bunch collisions) has already exceeded the design value by almost a factor of two. ZEUS has collected an integrated luminosity of over 500 nb^{-1} at the time of writing in mid-October, about 20 times that collected in 1992.

The proton current per bunch is limited to about one third of design, but should reach design current in 1994 after the installation of longitudinal and transverse feedback sytems in the pre-accelerator DESY III and in HERA, respectively. The design current per bunch for electrons has been achieved, although not routinely. In 1994 we expect another large increase in integrated luminosity, from increased currents per bunch, more bunches, shorter filling times and improved reliability of operation as this complex machine is better understood.

The performance of HERA to date strongly supports the belief that the full physics potential of ZEUS will be realized in the coming years.

1.3 The Status of ZEUS

The ZEUS detector, shown in figure 1, was designed to exploit the physics potential of HERA by emphasizing high precision tracking, hermetic calorimetry with the best possible energy resolution for hadrons and excellent electron and muon identification. Protons enter from the right and electrons from the left in the figure. The coordinate system, centred on the nominal interaction point, is defined with positive z along the proton direction and positive y upwards.

Charged particles are tracked by the inner tracking system, consisting of a vertex detector (VXD), a central cylindrical tracking detector (CTD), planar drift chambers in the forward and rear directions (FTD, RTD), and transition radiation detectors (TRD) in the forward direction. A thin superconducting solenoid surrounding the inner tracking system produces a magnetic field of 1.43 T in the centre. A uranium-scintillator calorimeter (FCAL, BCAL, RCAL) encloses the solenoid and inner tracking detectors. The magnetized iron yoke surrounding the calorimeter is instrumented for use as a backing calorimeter. Inside and outside of the yoke are large chambers for measuring muons (BMUON, RMUON). In the forward direction, iron toroids and additional tracking chambers (FMUON) improve the measurement of the forward going muons, which have high momentum.

The CAL, the CTD the VXD were the main central components used for the analysis leading to the physics results described below.

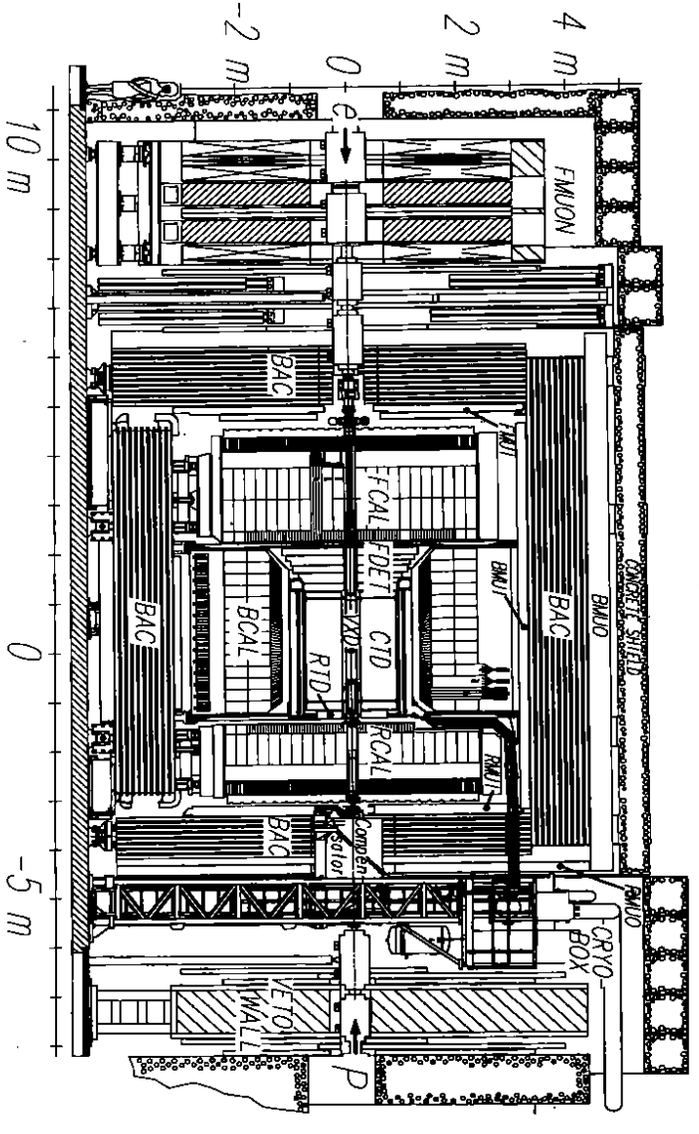

Figure 1: A side view of ZEUS.

The CTD has 9 superlayers (5 axial and 4 small angle stereo), each with 8 layers of sense wires read out by a high resolution FADC system. This FADC system was not ready in 1992, but was fully installed for the 1993 running. The three innermost axial layers (1, 3 and 5) are instrumented with z-by-timing electronics, mainly intended for triggering purposes. We used the z-by-timing information to reconstruct tracks in the 1992 data. With this electronics the z coordinate of a track 'hit' is measured with a resolution of about 4.5 cm from the difference in the time of arrival of pulses at each end of the wire, and the $r-\phi$ coordinate is measured with a resolution of about 900 μm. The FADC system has operated reliably in the 1993 running. Currently the spatial resolution is about 250 μm; this will improve steadily as the CTD calibration becomes better understood. The VXD gives 12 additional hits per track with a resolution down to 40 μm.

The calorimeter consists of three parts: RCAL covering the backward pseudo-rapidity range in the HERA reference frame ($-3.8 < \eta < -0.75$), BCAL covering the central region ($-0.75 < \eta < 1.1$), and FCAL covering the forward region ($1.1 < \eta < 4.3$). Scintillator tiles form towers that are longitudinally segmented into electromagnetic (EMC) and hadronic (HAC) cells. Characteristic transverse sizes are 5 cm $\times$ 20 cm for the EMC cells of FCAL and BCAL and 10 cm $\times$ 20 cm for those in the RCAL. The HAC cells are typically 20 cm $\times$ 20 cm in the transverse dimensions. Holes of 20 cm $\times$ 20 cm in the center of FCAL and RCAL accommodate the HERA beam pipe. The resulting solid angle coverage of the calorimeter is 99.7% of 4π.

The calorimeter readout provides precise energy and time measurements for the 5918 cells, each of which is instrumented with two photomultipliers. On average less than 0.1 percent of the cells are without operational readout. As measured in test beam conditions, the energy resolution is $18\%\sqrt{E}$ (E in GeV) for electrons and $35\%\sqrt{E}$ for hadrons. The timing resolution of the cells is $1.5/\sqrt{E} \oplus$ 0.5 ns.

It has been shown in test beams[1] that the calibration of the calorimeter can be maintained at the 1-2% level using the signal from the depleted uranium (DU) radioactivity. The DU calibration, which is monitored continuously, has been stable at the few percent level since the beginning of operational experience in ZEUS. The calorimeter noise, which is dominated by the uranium radioactivity, is typically 15 MeV in the EMC cells and 25 MeV in the HAC cells. A cut of 60 MeV for the EMC cells and 110 MeV for the larger HAC cells reduces the

influence of noise on the measurement of kinematic variables.

Inside the calorimeter is the Hadron Electron Separator (HES), a silicon pad (3×3 cm^2) system located at the depth of the electromagnetic shower maximum to improve electron identification. The RCAL has been partially equipped with the HES, although some of the readout electronics is missing. The RHES will be completed during the 1993/94 winter shutdown.

Close to the beamline downstream in the electron direction, photon and electron calorimeters (LUMI) are installed to determine the luminosity by measuring the rate of bremsstrahlung, $ep \rightarrow ep\gamma$. The LUMI detectors are also used in the physics processes of interest, the electron calorimeter to tag photoproduction events and the photon calorimeter to detect initial state radiation. A set of scintillation counters (C5) partially surrounds the beampipe behind the rear part of the calorimeter to measure the timing of both beams and to detect background events generated upstream of the detector by the proton beam. A further rejection of these background events is provided by the VETOWALL, two large planes of scintillator counters separated by a 1 m thick wall of iron. A small tungsten-silicon calorimeter (BPC) to tag electrons scattered with Q^2 up to 1 GeV^2 has been installed recently next to the beampipe in the region of the C5 counters.

Downstream of the main detector in the proton direction, a leading proton spectrometer (LPS) consisting of six measuring stations of silicon strip detectors is installed in the proton ring to detect forward scattered protons. About half of the detectors are installed and have been commissioned. A Forward Neutron Calorimeter (FNC) will also be installed to detect leading neutrons both in diffractive and charge exchange interactions. By measuring the latter reaction it should be possible at HERA to measure the DIS structure function of the pion. Already a prototype FNC has been operating in 1993 and we have observed high energy forward neutrons in many interesting events, including diffractive photoproduction and DIS rapidity gap events.

Further installation during the 1993/94 winter shutdown will include: the readout electronics for the FTD, RTD and TRD; the final RTD chamber (a prototype chamber is currently installed); the remaining silicon detectors of the LPS; and some further trigger electronics for the CTD.

The ZEUS detector has been functioning well with no serious problems. In 1993 the data taking efficiency, defined as the ratio of the luminosity recorded by ZEUS and that delivered by HERA, has ranged up to 90%, depending on the

beam conditions. A steady improvement in the efficiency of operation reflects the reliability of the subsystems and software.

1.4 Trigger

The high background and 96 ns bunch spacing makes triggering at HERA a challenging task. The major source of background, proton interactions with the residual gas and the beampipe, called beam gas, must be eliminated without losing efficiency for deep inelastic ep scattering and possible new physics processes with very low cross section. Not all of the large photoproduction cross section can be recorded, so the trigger system must select the more interesting sub-processes, such as hard scattering and heavy quark production. ZEUS has a three level trigger system, with increasing sophistication at each level. Because of the short time between bunch crossings, both the data and the trigger decision logic are pipelined at the first level to avoid deadtime. The second level trigger uses a network of transputers. At the third level, full event reconstruction is performed in a 1000 MIP farm of commercial RISC computers (SGI 35S).

In 1992 the trigger was quite loose. We triggered on an energy deposit above a threshold in calorimeter trigger towers of 20×40 cm^2. A photoproduction trigger used the same calorimeter trigger, but with lower thresholds, and required a scattered electron in the LUMI detector. Events were rejected if the timing in the C5 counters or the RCAL was consistent with an upstream beam gas interaction. Particles from such events arrive at the RCAL about 10 ns before particles from ep interactions.

In 1993, with higher luminosity, the trigger requirements are more stringent at all 3 levels. We trigger on the total transverse energy E_T, missing E_T and combinations of tracking and calorimeter energy information at the first and second levels, make tight timing cuts at the second and third levels and run many physics filters at the third level.

The excellent timing resolution of the CAL is one of the most powerful tools we have to reject proton beam gas background. Even tighter cuts on the time are made in a more refined analysis in the offline physics filters.

2 Photoproduction at HERA

2.1 Introduction

The high center of mass energy of HERA allows the study of photoproduction in a very wide energy range up to γp center of mass energies $W_{\gamma p} = 250$ GeV in a single experiment. The photoproduction topics covered in this talk are:

- total and partial photoproduction cross sections,
- high mass diffractive photoproduction,
- elastic photoproduction of ρ-mesons,
- jets in photoproduction and the separation of direct and resolved processes.

Photoproduction at HERA is measured using the interactions of quasi-real photons on protons in the reaction $ep \to e' + \gamma^* p \to e' + X$. The quasi-real photon γ^* is either tagged by measuring the scattered electron e' in the small angle LUMI electron calorimeter or it escapes undetected. The tagging range is from 150 GeV to 250 GeV in $W_{\gamma p}$ and from the kinematic minimum $Q^2_{\rm min}$ of about 10^{-8} GeV^2 to the acceptance limit $Q^2_{\rm max} = 0.02$ GeV^2. The value of $y = (E_e - E_{e'})/E_e$ and the center of mass energy $W_{\gamma p} = \sqrt{4yE_eE_p}$ are obtained from the electron beam energy E_e, the proton beam energy E_p, and the energy of the scattered electron $E_{e'}$. For untagged events, the Q^2 range is from $Q^2_{\rm min}$ to about 4 GeV^2, above which the electron is accepted by the ZEUS calorimeter, and $W_{\gamma p}$ is obtained from the hadronic system measured in the main calorimeter by $W_{\gamma p} = \sqrt{4y_{\rm JB}E_eE_p}$. Here $y_{\rm JB} = \sum_i (E_i - p_{zi})/2E_e$ is the Jacquet-Blondel estimator of y. The sum runs over all calorimeter cells i, E_i is the energy deposited in the calorimeter cell i, and p_{zi} is its projection on the proton direction. The cell angles are calculated from the geometric center of the corresponding cell and the event vertex.

To relate the ep cross section to the γp cross section we use the Weizsäcker-Williams approximation:

$$\frac{d\sigma_{ep}}{dy} = \frac{\alpha}{2\pi}\left[\frac{1+(1-y)^2}{y} \cdot \ln\left(\frac{Q^2_{\rm max}}{Q^2_{\rm min}}\right) - \frac{2(1-y)}{y} \cdot \left(1 - \frac{Q^2_{\rm min}}{Q^2_{\rm max}}\right)\right] \cdot \sigma^{\gamma p}_{tot}(W_{\gamma p}).$$

2.2 Total and Partial Photoproduction Cross Sections

A tagged photoproduction trigger selects photoproduction events with high efficiency. It requires an energy deposit > 5 GeV in the LUMI electron calorimeter

in coincidence with energy in the CAL, either > 0.46 GeV in any electromagnetic trigger tower, or > 1 GeV in any hadronic trigger tower of the RCAL, excluding the towers around the beam pipe, where the threshold was raised to 2.5 GeV. It also required no hit in veto counters, due to upstream proton gas interactions.

In the offline analysis we require:

- between 15.2 GeV and 18.2 GeV energy deposited in the LUMI electron calorimeter, thus selecting $W_{\gamma p}$ between 167 and 194 GeV,
- > 0.7 GeV energy deposited in the RCAL, with a timing in the calorimeter incompatible with a proton gas interaction,
- < 1 GeV energy deposited in the photon calorimeter of the luminosity detector to reject radiative events,
- no reconstructed cosmic ray muon,
- statistical subtraction of electron beam gas events using the electron pilot bunches,
- statistical subtraction of accidental coincidences of proton beam gas events and electron bremsstrahlung events.

For an integrated luminosity of 13.0 ± 0.6 nb^{-1}, the selected data sample is 5963 events. The energy distributions in the individual calorimeter sections and the transverse energy distribution show that the data fall into two classes: events with essentially zero energy in the forward and central calorimeters FCAL and BCAL, as expected for photon and proton diffractive events, and events with energy distributed over the entire angular range of the detector, as expected for non-diffractive events.

To describe the data we classify photoproduction according to the following subprocesses:

- elastic vector meson production $\gamma p \to Vp$, where $V = \rho, \omega, \phi$ are the low-mass vector mesons; for practical reasons we include higher vector mesons V in the diffractive processes defined below,
- single diffraction dissociation of the proton $\gamma p \to VX$,
- single diffraction dissociation of the photon $\gamma p \to Xp$, where X also includes the high mass vector mesons,
- double diffraction disociation $\gamma p \to X_1 X_2$,

- non-diffractive $\gamma p \to X$.

The following strategy is used to obtain the acceptances of the different subprocesses, their fractional cross sections and finally the total cross section. The acceptance of the photon tagging and of the main detector are treated separately; this assumes that all subprocesses have the same Q^2 and $W_{\gamma p}$ dependence in the kinematic range considered. The acceptance of the photon tagging is obtained from a Monte Carlo calculation; it is cross checked by high statistics data from the reaction $ep \to e\gamma p$. Radiative corrections are taken from a Monte Carlo study, which is verified with experimental data. For the acceptance of the hadronic system we use a variety of models to generate Monte Carlo events and pass them through the ZEUS program chain for detector simulation, trigger simulation and event reconstruction. A χ^2-comparison of experimental data and Monte Carlo simulated data for the different models and model parameters allows us to determine the fractional cross sections and acceptances compatible with the experimental data, and finally the acceptance-corrected number of measured events. Combining the corrected number of events with the photon flux for the given luminosity gives the total and the partial photoproduction cross sections.

The models used to generate non-diffractive events were PYTHIA,[2] where the structure function of one of the hadrons was replaced by a parametrization of the photon structure function, a superposition of π^+ and π^- proton interactions in HERWIG,[3] models based on parametrizations of multiplicity and p_T distributions, models with phenomenological QCD parton dynamics, models simulating γp interactions as the sum of a non-perturbative soft component and a perturbative QCD mini-jet component. To generate the different classes of diffractive events, we used PYTHIA or HERWIG for elastic vector meson production, PYTHIA for the single diffraction reaction $\gamma p \to VX$, PYTHIA, a modified version of HERWIG or the Nikolaev-Zakharov[4] model for the single diffractive reaction $\gamma p \to Xp$, and PYTHIA for the double diffraction reaction $\gamma p \to X_1 X_2$.

We perform the analysis separately for the two data samples $E_{\mathrm{FCAL}} < 1$ GeV and $E_{\mathrm{FCAL}} > 1$ GeV, which provides a quite clean separation of diffractive and non-diffractive events.

The analysis shows that most of the models provide a good description of the data, and that the acceptances can be well constrained. The acceptance for the non-diffractive events in the $E_{\mathrm{FCAL}} > 1$ GeV sample lies between 0.83 and 0.95.

The acceptances for diffractive subprocesses in the $E_{\rm FCAL} > 1$ GeV sample are: 0.31 ± 0.05 for $\gamma p \to Vp$, 0.46 ± 0.05 for $\gamma p \to VX$, 0.80 ± 0.05 for $\gamma p \to Xp$, and 0.82 ± 0.03 for $\gamma p \to X_1 X_2$.

The separation between low mass vector meson production and photon diffractive dissociation is obtained from the characteristic energy distribution in the RCAL – the decay products of the low mass vector mesons barely reach the calorimeter and cluster around the beam pipe, whereas the photon diffractive events produce a more widely spread distribution.

The separation between elastic and diffractive low mass vector meson production assumes that the two single diffractive processes, photon- and proton-diffraction, have similar cross sections and about twice the cross section of the double diffractive dissociation process. This could be checked, however with big errors, by determining the fraction of diffractive events in the $E_{\rm FCAL} > 1$ GeV sample. These uncertainties result in the large error for the cross section of elastic low mass vector meson production, but have, however, a fairly small effect on the total cross section.

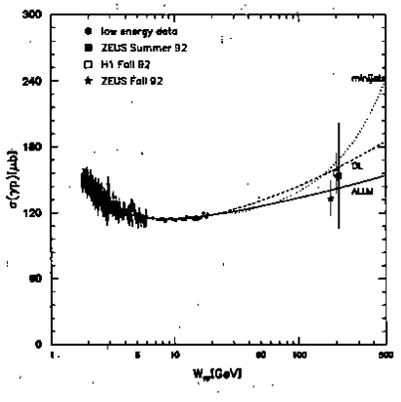

Figure 2: Total photoproduction cross section as function of the γp center of mass energy $W_{\gamma p}$. The solid line is the prediction of the ALLM[8] parametrization, the dashed line is that of DL[9], and the dotted line uses the DG[11] parametrization for the photon with $p_{\rm T}^{\rm min} = 2$ GeV/c.

From the overall acceptance corrected number of events, the integrated luminosity, and the photon flux integrated over the accepted Q^2 and y ranges, the total average photoproduction cross section for $W_{\gamma p}$ between 167 and 194 GeV is obtained:

$$\sigma_{tot}(\gamma p) = 133 \pm 2.5(\text{stat.}) \pm 16(\text{syst.})\mu\text{b}$$

The following effects contribute to the sytematic error: the acceptance uncertainty of the main detector (7.4%), the acceptance uncertainty of the tagging system (7.8%) and the luminosity uncertainty of (4.6%). These have been added in quadrature to give the overall systematic error. In figure 2 the total cross section is compared to the measurement from H1,[5] from ZEUS,[6] data from lower energies,[7] and theoretical extrapolations[8–10] to the HERA energy. The data, with the present errors is able to exclude models which predict a dramatic rise, and is compatible with more conventional extrapolations.

The values for the photoproduction partial cross sections are: inelastic non-diffractive $\sigma_{nd}(\gamma p) = 88 \pm 11\mu$b, diffractive $\sigma_d(\gamma p) = 31 \pm 8\mu$b, and elastic $\sigma_{el}(\gamma p) = 14.2 \pm 5.4\mu$b. The errors quoted on the partial cross sections include statistical and systematic errors added in quadrature.

Assuming further that the ρ^0 contributes 87% of the elastic cross section, we obtain the following cross section for elastic ρ production: $\sigma(\gamma p \to \rho^0 p) = 12.3 \pm 4.6\mu$b.

These first measurements of partial photoproduction cross sections at HERA energies agree well with theoretical extrapolations from lower energy data.[12]

2.3 High Mass Diffractive Photoproduction

Given the high center of mass energy, HERA is an ideal tool to study photon diffraction over a wide range of M_X, the mass of the diffractive system. To illustrate the selection of photon diffractive events, we show in figure 3 the distribution of $\eta_{\rm max}$, the maximum pseudorapidity of the calorimeter condensates in the tagged photoproduction events. A condensate is a group of contiguous calorimeter cells with energies above 0.06 GeV in the electromagnetic and above 0.11 GeV in the hadronic sections, and a total condensate energy > 0.4 GeV. The pseudorapidity $\eta = -\ln(\tan(\theta_{\rm cond}/2))$ is calculated in the laboratory system where η = -3.8 corresponds to the calorimeter limit in the electron direction, and η = 4.3 to the calorimeter limit in the proton direction. For the typical tagged photon energy of

10 GeV, 90° in the γp center of mass system corresponds to $\eta = 2.2$. The data fall into two classes, a large peak of $\eta_{\max}$ in the range 3–6 mainly consisting of non-diffractive events and described by a non-diffractive Monte Carlo simulation (solid line) and photon diffractive and vector meson production for $\eta_{\max} \leq 2$. We call the events with $\eta_{\max} < 2$ photon diffractive, as they do not show any activity in the proton direction. Figure 4 shows the dN/dM_X^2 distribution for these events. Values of M_X^2 well above 100 GeV^2 are produced. The data is not corrected for acceptance, and the selection cuts strongly suppress high values of M_X. A detailed analysis is under way to study the properties of high mass photon diffraction.

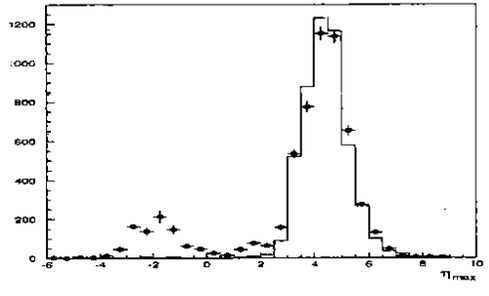

Figure 3: $\eta_{\max}$ for tagged photoproduction. The dots are the data and the solid line is a Monte Carlo simulation of non-diffractive events.

2.4 Elastic Photoproduction of ρ mesons

The energy of tagged photons is between 10 GeV and 20 GeV. Elastically produced ρ mesons at small Q^2 carry essentially the total photon momentum. Due to the high ρ momentum, the decay angles of the pions relative to the photon direction are small and they miss the CTD or even stay within the beam pipe. Thus an untagged ρ trigger has been introduced for the 1993 running, which requires $\geq$ 1 track in the CTD, $>$ 0.46 GeV in the REMC and $<$ 3.75 GeV in the towers around the beam pipe in the FCAL to veto the strong proton gas background. Again, the trigger required no hit in the veto counter.

This trigger, with the additional requirement that both tracks are reconstructed in the CTD, accepts elastically produced ρ mesons in the energy range

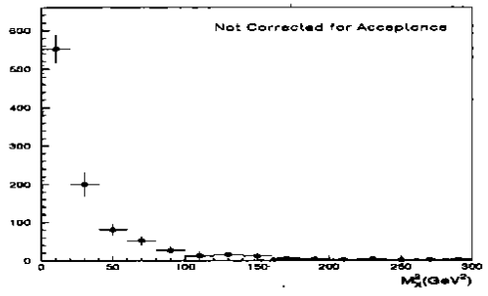

Figure 4: Mass squared of the diffractive system (cut $\eta_{\max} < 2$) for tagged photoproduction.

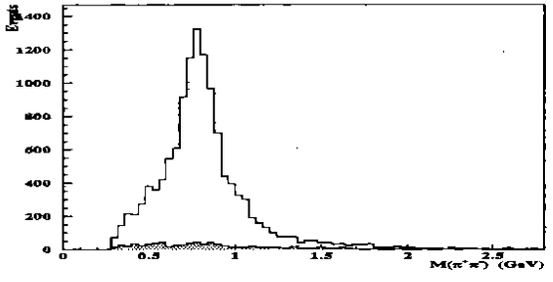

Figure 5: $M_{\pi^+\pi^-}$ for untagged photoproduction. (Shaded histogram for same sign particles.)

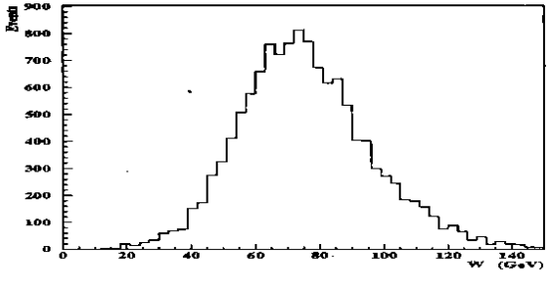

Figure 6: $W_{\gamma p}$ for untagged ρ photoproduction.

$W_{\gamma p}$ between 30 GeV and 110 GeV. The maximum acceptance is about 20% at 70 GeV. Other vector mesons like ω mesons or ρ' mesons, and photon diffractive production also have good acceptances. For events with only two oppositely charged particles in the CTD we show in figure 5 first results for the effective mass spectrum, assuming that the two particles are pions. The $W_{\gamma p}$ distribution, assuming elastic production, is shown in figure 6. The data demonstrate that a high statistics study of ρ production is feasible at HERA.

2.5 Hard Photoproduction

At large centre of mass energy and small values of Q^2 we expect to see evidence of hard collisions between quasi-real photons and partons from the proton. Because of its dual nature, the photon can interact either directly with a gluon (boson gluon fusion) or a quark (QCD Compton scattering) in the proton, or it can interact in a resolved process, in which its constituents interact with the constituents of the proton.[13] These hard interactions will thus reveal the internal structure of the photon and allow the extraction of the parton densities of the photon.[14] An important first step is the identification and measurement of photoproduction events with hard subprocesses. The signature is a final state with well defined jets of hadrons.

Jets are identified by searching for localized clusters of energy deposits in pseudorapidity (η) - azimuth (ϕ) space,[15] using a cone radius of $R = \sqrt{\Delta\phi^2 + \Delta\eta^2} = 1$. In order to exclude effects of the poorly understood proton remnant, we look for jets with total transverse energy $E_T > 5$ GeV and $\eta < 1.6$ ($\theta > 23°$).

ZEUS has observed a clear signal for jet production in γp interactions.[16] One spectacular event is shown in figure 7, where two jets are visible, each having an energy of 30 GeV, as well as part the proton remnant. Since no energy is deposited in RCAL, where one would expect the fragments of the photon remnant in a resolved contribution, this event is a candidate for a direct photon interaction.

Clear evidence for the resolved process can be seen in the characteristics of the two-jet event sample. In figure 8 the energy deposited in RCAL is plotted against the pseudorapidity, $\eta_{\min}$, of the most backward jet. For $\eta_{\min} > 0$ both jets point in the forward direction and therefore contribute no energy to RCAL. Nevertheless, there are many events with $\eta_{\min} > 0$ and a large amount of energy in the RCAL. This substantial RCAL energy is explained as the the remnant of the photon in

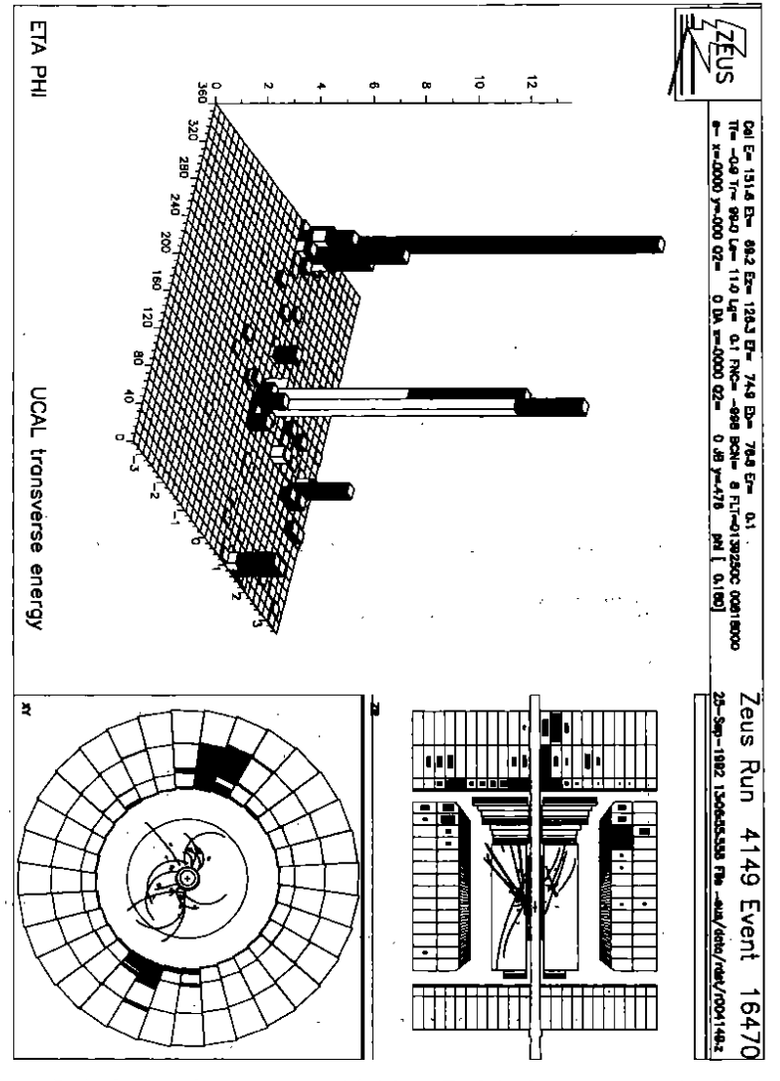

Figure 7: A photoproduction event with 2 jets. Each jet has an energy of 30 GeV. This event is a candidate for a direct photon interaction since there is no evidence of a photon remnant in the RCAL.

the resolved photon process.

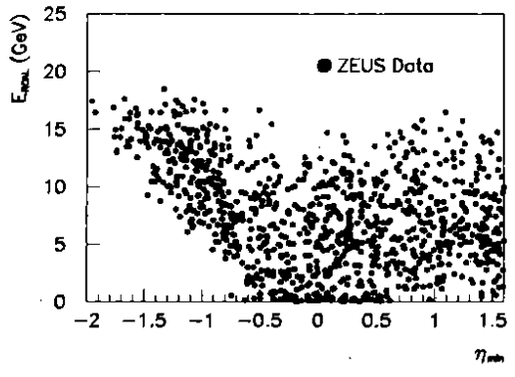

Figure 8: The energy deposited in RCAL plotted against the pseudorapidity, $\eta_{\rm min}$, of the most backward jet.

The distribution of transverse energy $E_{\rm T}$ of the photoproduced jets is shown in figure 9. Jets with $E_{\rm T}$ up to 19 GeV are seen. The predictions of the HERWIG Monte Carlo program, normalized to the data, are superimposed; the shape of the data is described well. The relative contributions of the resolved and direct processes in the Monte Carlo siimulation are also shown.

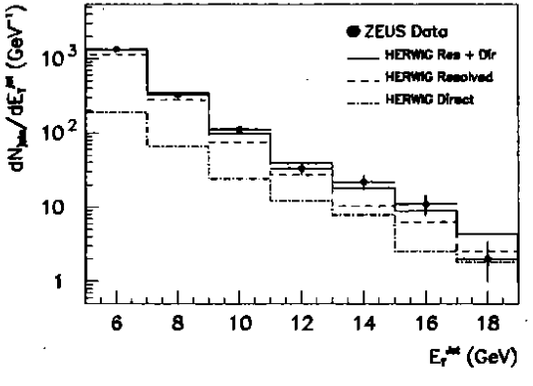

Figure 9: The distribution of transverse energy for inclusive jets.

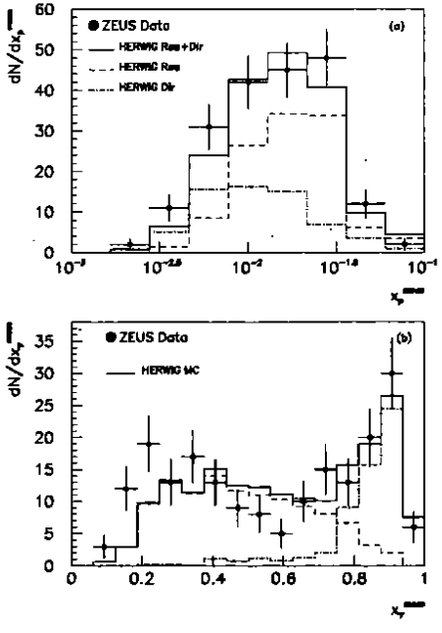

Figure 10: Kinematic distributions for events with two or more jets. (a) x_p^{meas} distribution for the final sample. (b) x_γ^{meas} distribution for the final sample.

The fraction of one-jet, two-jet and three-jet events in the sample is 6.5%, 1.4% and 0.1%, respectively. From a measurement of the energies and angles of the jets in the two-jet sample, we can estimate the fractions of the momenta of the proton and photon carried by the interacting partons. We can approximate these, x_p and x_γ, as

$$x_p^{meas} = \frac{\sum_{jets}(E+p_Z)}{2E_p}, \qquad x_\gamma^{meas} = \frac{\sum_{jets}(E-p_Z)}{\sum_{CAL}(E-p_Z)}.$$

The distribution of these variables in the two-jet sample is shown in figure 10. From Monte Carlo studies it was found that imposing the requirements $|\eta^{jet_1} - \eta^{jet_2}| \leq 1.5$ and $|\phi^{jet_1} - \phi^{jet_2}| \geq 120°$ improves the resolution in x_γ^{meas} and these cuts have been applied. The resolved process MC is in reasonable agreement with the data towards low x_γ^{meas}, but cannot account for the large peak at 0.9. The direct process MC, however, predicts a peak at 0.9, in agreement with the data. This is the first unambiguous evidence for direct photon interactions in photoproduction.

3 Deep Inelastic *ep* Scattering

The deep inelastic neutral current scattering (NC-DIS) of an electron off the proton is viewed in the quark parton model (QPM) as a point-like interaction of the virtual photon emitted from the electron with a quark originating from the proton. This is schematically depicted in figure 11. The kinematical variables used to describe this process expressed in terms of the four-momenta of the incoming electron k, the scattered electron momentum k' and the incoming proton P are:

- $Q^2 = -q^2 = -(k-k')^2$, the negative of the four-momentum transfer squared between initial and final state electrons,
- $x = \frac{Q^2}{2P\cdot q}$, the Bjorken variable identified with the fraction of proton momentum carried by the struck quark,
- $y = \frac{P\cdot q}{P\cdot k}$, the fractional energy transfer to the proton in its rest frame,
- $W^2 = (xP+q)^2 = Q^2\frac{1-x}{x} + m_p^2$, the center of mass energy of the $\gamma^* p$ system, where m_p is the mass of the proton.

As ZEUS is a hermetic detector, the kinematic variables can be determined either from the scattered electron, from the hadronic final state or from a combination of the two. We use the so called double angle method[17] (DA), in which $x_{\rm DA}$

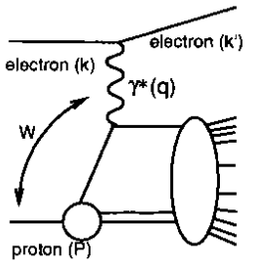

Figure 11: Schematic diagram describing deep inelastic electron proton scattering

and $Q^2_{\rm DA}$ are derived from the angle of the scattered electron θ_e and the angle γ_h, which represents the production angle of a massless object – the scattered quark in the QPM – balancing the transverse momentum and the $E-p_z$ of the electron:

$$\cos\gamma_h = \frac{(\sum_i p_{xi})^2 + (\sum_i p_{yi})^2 - (\sum_i (E_i - p_{zi}))^2}{(\sum_i p_{xi})^2 + (\sum_i p_{yi})^2 + (\sum_i (E_i - p_{zi}))^2}\ .$$

The sum runs over all particles excluding the scattered electron. In determining $\cos\gamma_h$ in the experiment the sum over particles is replaced by the sum over all cells of the calorimeter excluding those assigned to the electron. The proton fragments which are not detected in the calorimeter have a negligible influence on the determination of γ_h. In order to retain sufficient accuracy in the calculation of the angle γ_h, we require the Jacquet-Blondel estimator of y to be greater than 0.04.

Figure 12 shows a text book example of a high Q^2 NC-DIS event measured in the ZEUS detector. Its kinematical variables are $x = 0.07$ and $Q^2 = 2.5\cdot 10^3$ GeV^2. So far the highest Q^2 event in the NC sample has $Q^2 = 21.5\cdot 10^3$ GeV^2 and $x = 0.28$. In a data sample of 300 nb^{-1} we have observed 11 charged current events with $Q^2 > 1\cdot 10^3$ GeV^2, the highest Q^2 event having $Q^2 = 14\cdot 10^3$ GeV^2 and $x = 0.44$.

The cross section for NC-DIS is expressed in terms of the proton structure functions. In the most general case there are three structure functions. In the region where the photon exchange dominates – for Q^2 much smaller than the intermediate bosons mass squared – the cross section depends only on two structure functions:

$$\frac{d^2\sigma}{dx\,dQ^2} = \frac{2\pi\alpha^2(1+(1-y)^2)}{xQ^4}\left[F_2(x,Q^2) - \frac{y^2}{1+(1-y)^2}F_L(x,Q^2)\right](1+\delta_r(x,Q^2))\ .$$

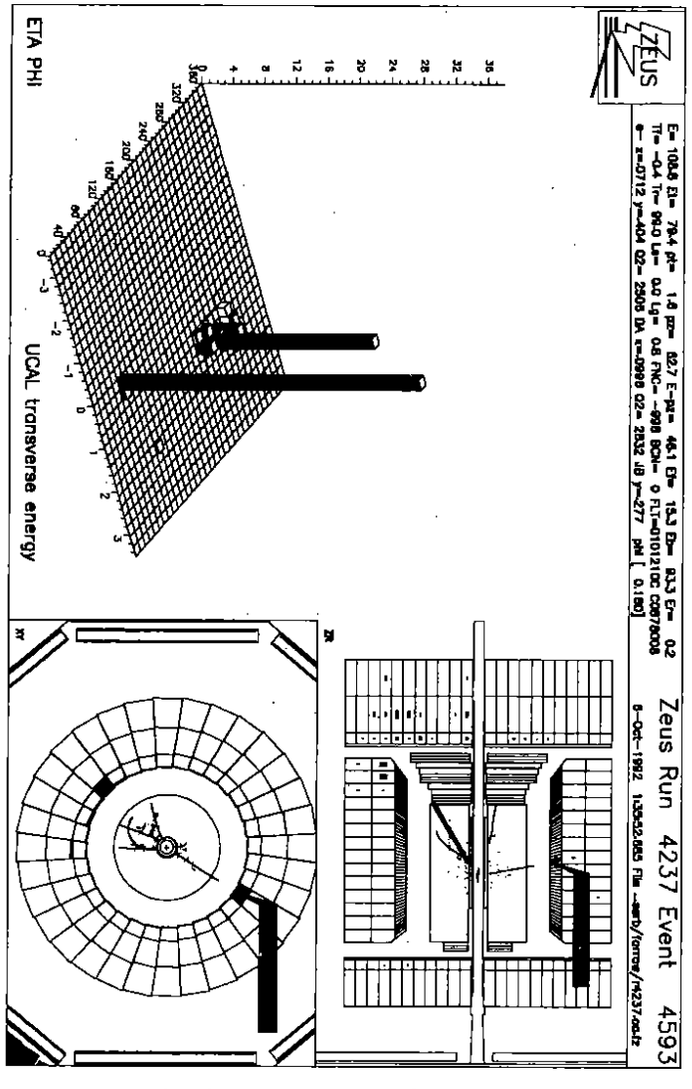

Figure 12: A NC-DIS event with a 39.7 GeV electron scattered into the BCAL and a jet balancing p_T on the opposite side. This event has $Q^2 = 2500$ GeV^2 and $x = 0.07$.

F_2 is proportional to the total absorption cross section of virtual photons, F_L is proportional to the absorption cross section of longitudinally polarized photons and δ_r is an overall correction due to QED radiative effects. In the quark parton model the structure function F_2 can be expressed in terms of parton distributions in the proton. For spin $\frac{1}{2}$ partons $F_L = 0$. QCD radiation introduces corrections to this simple picture and beyond the leading logarithmic approximation $F_L \neq 0$. With 25 nb^{-1}, due to the photon propagator effect, the exchange of the photon is the dominant process in our DIS event sample.

3.1 Selection of the DIS Sample

In the ZEUS experiment we define an ep interaction as being due to deep inelastic scattering if the scattered electron enters the geometrical acceptance of the CAL. This corresponds roughly to $Q^2 > 4$ GeV^2. In our selection of DIS events we thus require the presence of an identified electron in the calorimeter with energy larger than 5 GeV. Below that cut the efficiency and purity of the electron finder algorithm is low. In order to achieve a full containment of the electron shower and a good position resolution, we require the electron impact point to be located outside a 16×16 cm^2 box centered on the beam axis. Spurious low energy electrons, especially in the forward direction, are removed by requiring that y determined from the electron be less than 0.95.

From energy-momentum conservation we expect

$$\delta \equiv \sum_i (E_i - p_{zi}) = 2E_e$$

where E_i and p_{zi} are the energy and z momentum component of particle i respectively, E_e is the energy of the incoming electron and the sum runs over all the particles present in the final state, including the scattered electron. In the experiment δ is estimated using the information from the calorimeter cells. To each cell above the noise cut a momentum vector is assigned, using the deposited energy and the angle of the cell, as seen from the reconstructed vertex position. Only events with $\delta > 35$ GeV are kept. This cut reduces substantially the backgrounds from proton gas interactions and from photoproduction, with the electron escaping through the beam pipe and a wrongly identified electron. It also rejects DIS events with a hard photon radiated in the initial state, diminishing thereby the influence of radiative corrections. The proton fragments escaping detection

through the beam pipe in the proton direction do not contribute to δ.

After all these selection cuts and after removing cosmic muons and elastic QED Compton events, we remain with 2012 events. The contamination of electron-beam gas interactions in this sample is small and can be estimated from the unpaired electron bunches. The remaining contamination from photoproduction processes has been estimated using a sample of events generated with the PYTHIA Monte Carlo program, tuned to reproduce best our data. In the region of $Q^2 > 10$ GeV^2 the total contamination is estimated to be 35 events with 25 originating from the photoproduction background.

3.2 Determination of the Proton Structure Function F_2

The extraction of F_2 proceeds in two steps. First the cross section is corrected for acceptance and migration of events from their 'true' (x, Q^2) to the reconstructed $(x_{\rm DA}, Q^2_{\rm DA})$. The corrections are determined from a full Monte Carlo simulation of DIS scattering in the ZEUS detector.

Neutral current DIS events with $Q^2 > 2$ GeV^2 were generated using the HERACLES[18] program, which includes first order electroweak radiative corrections. The hadronic final state was simulated using the color-dipole model[19] as implemented in ARIADNE[20] for the QCD cascade, and JETSET[21] for the soft hadronization. For the parametrizations of the parton density distributions we used the MRS D'_ set.[22]

The comparison of the data sample with the equivalent Monte Carlo sample, normalized to the data is presented in figure 13. A good overall agreement is observed. This allows us to determine bin to bin corrections due to acceptance and migration. The fiducial cut imposed on the impact point of the scattered electron in the calorimeter requires large acceptance corrections for $Q^2 < 10$ GeV^2. We thus limit the analysis to the region of $Q^2 > 10$ GeV^2.

The events are binned in $x_{\rm DA}$ and $Q^2_{\rm DA}$ with bin sizes compatible with the respective resolutions. The relative resolution in $Q^2_{\rm DA}$ is 25%, independent of $Q^2_{\rm DA}$. The relative resolution in $x_{\rm DA}$ varies smoothly with $x_{\rm DA}$, from 25% for $x_{\rm DA} = 10^{-2}$, to 80% for $x_{\rm DA} = 5 \cdot 10^{-4}$. For the further analysis we retain only bins for which the correction factors range from 0.8 to 1.9. A total of 1299 events remains in the selected bins. The estimated background is subtracted bin by bin.

In the second step the structure function F_2 is determined by comparing the

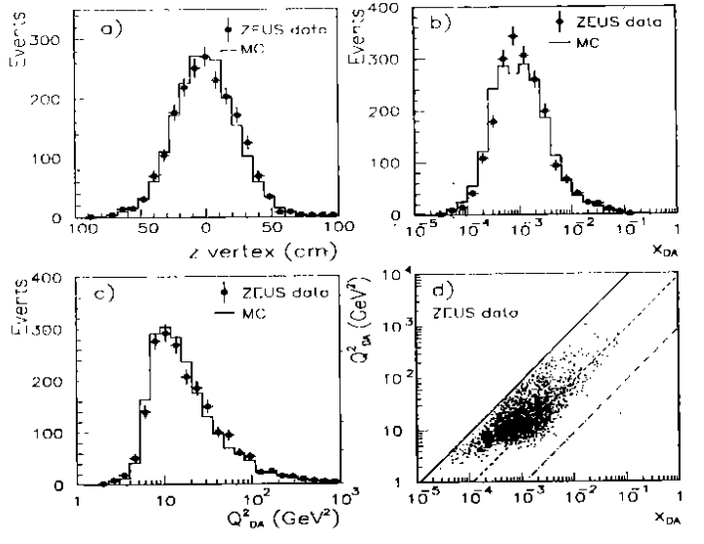

Figure 13: Comparison of data and Monte Carlo events samples: (a) the reconstructed vertex distributions, (b) the $x_{\rm DA}$ distribution, (c) the $Q^2_{\rm DA}$ distribution. The number of Monte Carlo events is normalized to the number of data events. (d) Distribution of events in the (x, Q^2) plane; the solid line corresponds to $y = 1$, the dashed line to $y = 0.1$ and the dot-dashed line to $y = 0.01$.

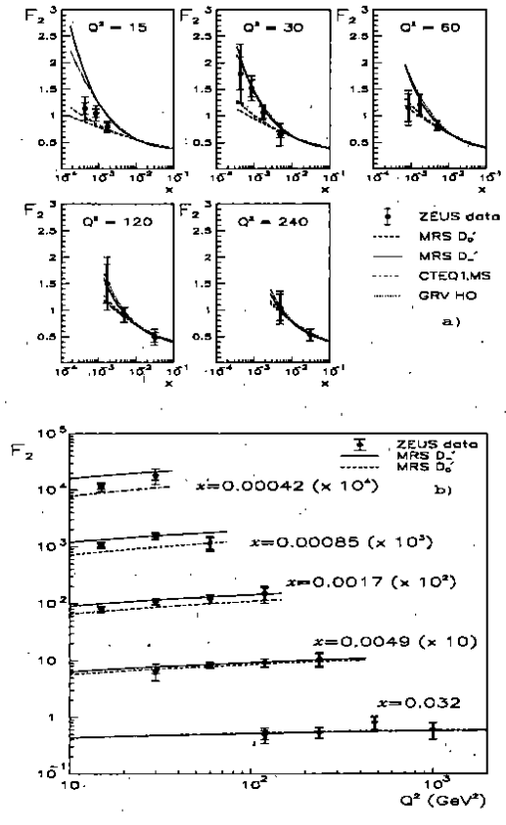

Figure 14: a) The structure function F_2 as a function of x for Q^2 values (in GeV^2) as denoted on the figure. b) The structure function F_2 as a function of Q^2 for different values of x as denoted on the figure. The inner error bar is the statistical error, and the outer bar shows the systematic error added in quadrature. The overall normalization uncertainty of 7% is not included. Also shown are several structure function expectations. (For H1 results see reference[26].)

measured cross sections to the ones obtained from the Monte Carlo sample, which includes radiative corrections. The correction due to F_L is calculated assuming the MRS D$'_-$ parametrization of parton distributions in the proton. For the double angle method used in this analysis, combined with the δ cut of 35 GeV, the radiative corrections are $\lesssim$10%. The largest correction for the F_L contribution amounts to 12%.

Possible sources of systematic errors were classified into several categories: photoproduction background, electron energy scale, hadron energy scale, electron position, hadron angle, vertex determination, CAL noise, QED radiation, structure function parametrizations and different reconstruction and unfolding methods. The systematic errors from each category were added in quadrature. The bin-by-bin systematic errors range from 5% to 30% (the latter in the high y region), and are to be compared to typical statistical errors of 10%. In addition there is an overall normalization uncertainty of 7%, of which 5% is from the luminosity determination and 5% is from the trigger efficiency and acceptance determination.

Figure 14 presents the results on F_2.[23] At fixed Q^2, F_2 rises significantly at small x values, increasing typically by more than a factor of two as x decreases from $x = 10^{-2}$ to the lowest measured value of $4.2 \cdot 10^{-4}$. The results are compared to a representative choice of existing parton parametrizations.[22,24,25] The Q^2 dependence of F_2 at fixed values of x is in agreement with scaling violation expected from perturbative QCD.

3.3 Final Hadronic States

In the quark parton model (QPM) the final hadronic state of a DIS ep scattering consists of a jet of particles originating from the struck quark, the so called current jet, and of particles originating from the remnant of the proton. The transverse momentum of the scattered electron is balanced by the current jet, while the proton remnant carries relatively little transverse momentum. QCD introduces substantial corrections to this simple picture. The phase space between the current jet and the proton remnant is filled by particles materializing from gluon radiation created by the color transfer between the struck quark and the remnant of the proton.

This effect is clearly observed at HERA, in particular at low x, where the

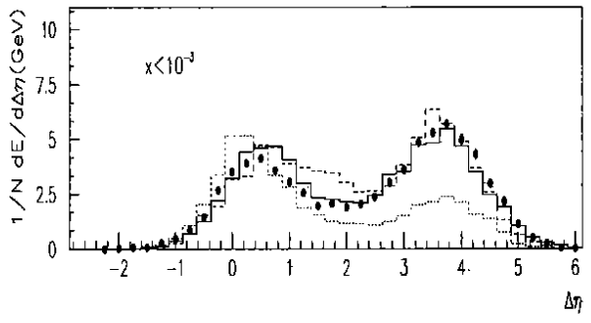

Figure 15: The energy weighted pseudorapidity $\Delta\eta$ of the hadronic system with respect to the struck quark from the quark-parton model. The ZEUS data points are shown as the dots. The dashed histogram is the result obtained with the ARIADNE Monte Carlo, the full histogram is ARIADNE with the addition of the boson gluon fusion diagram, and the dotted histogram is the Lund string fragmentation with parton showers evolved with a scale $Q^2(1-x)$.

rapidity separation between the current jet and the proton remnant is large. This can be seen in figure 15 where, for events with $x < 10^{-3}$ and $Q^2 > 10$ GeV^2, the energy weighted pseudorapidity distribution of the hadronic system is plotted relative to the pseudorapidity of the struck quark in the QPM. A clear two peak structure is observed. At large $\Delta\eta$ we observe the energy flow of the proton remnants while close to $\Delta\eta = 0$ we observe the decay products of the current jet. The peak of the current jet energy flow is slightly shifted from 0, an effect expected in QCD due to the extra parton radiation in the perturbative phase of the fragmentation process. It is reproduced by those fragmentation models which include explicitly higher order QCD corrections (see[27] for details).

Higher order QCD effects are directly observed at HERA in the form of multi-jet events.[28] Already at the scanning level clear evidence for two- and three-jet events is found.

We have studied the rate of multi-jet events by applying the JADE clustering algorithm, which assigns particles to the same jet if their invariant mass $m_{j_1 j_2} < y_{\rm cut} W$. The parameter $y_{\rm cut}$ controls the separation of jets. Monte Carlo studies show that such a definition of jets is little affected by hadronization effects. The

observed decrease of the two-jet rate with Q^2 is consistent with QCD expectations. A high statistics sample will eventually allow the determination of the running of the coupling constant α_S from a single experiment over a wide Q^2 range.

3.4 Large Rapidity Gap Events

Among the selected DIS events we observe a class of events whose characteristics are different from the ones described above. They do not show any hadronic activity in the calorimeter in the forward region, the region of the proton remnant. In order to quantify this effect, we define the variable $\eta_{\rm max}$ as the pseudorapidity of the calorimeter cluster of at least 400 MeV and the smallest production angle relative to the initial proton direction. The distribution of $\eta_{\rm max}$ for all the selected DIS events with $Q^2 > 10$ GeV^2 compared to the expectations from the DIS Monte Carlo simulation is presented in figure 16a.

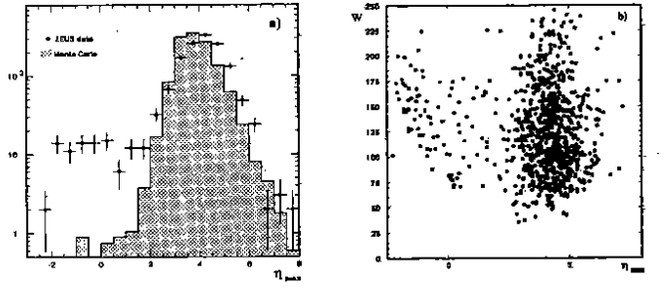

Figure 16: a) $\eta_{\rm max}$ distribution for data and Monte Carlo. b) Correlation between W and $\eta_{\rm max}$ in the data

A clear excess of events with small $\eta_{\rm max}$ is observed in the data over the Monte Carlo expectations. Fig. 16b shows that for these events W and $\eta_{\rm max}$ are correlated, which is not observed for the bulk of the events. This suggests different production mechanisms.

After subtracting the background from standard DIS (4 events) and from electron-beam gas interactions ($\leq$ 10 events) we are left with a signal of 78 $\pm$ 10 large rapidity gap events with $\eta_{\rm max} < 1.5$.[29]

Events with a large rapidity gap are expected if the interaction of the virtual

photon with the proton occurs through the exchange of a colorless object like the Pomeron. The nature of the Pomeron has been studied in the language of perturbative QCD by many authors.[30–37] The notion of the partonic structure of the Pomeron was first proposed by Ingelman and Schlein[38] and the observation of high p_T jets in diffractive $p\bar{p}$ interactions by the UA8 Collaboration[39] gave a strong support to such a concept.

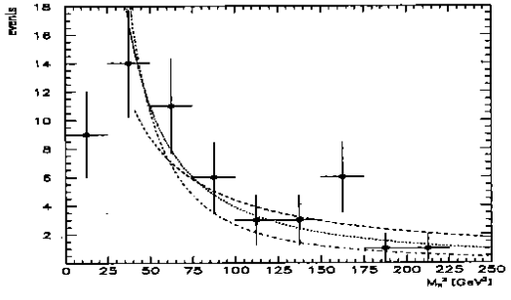

Figure 17: Distribution of M_X^2 for events with a large rapidity gap, $\eta_{max} < 1.5$ and $W_{DA} > 150$ GeV, uncorrected for acceptance and resolution effects. The dashed line shows a $1/M_X^2$ dependence, the dotted line – $1/M_X^3$, the dashed–dotted line – $1/M_X^4$.

In DIS, events due to the exchange of a Pomeron consist of a quasi-elastically scattered proton well separated in rapidity from the rest of the hadronic system. In this picture the rapidity gap increases with increasing W, which is seen in figure 16b. The ratio of the number of events with a large rapidity gap to the total number of events is within errors constant in the region $W > 150$ GeV, where acceptance corrections have little dependence on W. Also in this picture the distribution of the diffractively excited system M_X^2 is expected to fall off with M_X^2, as observed in fig. 17. The large rapidity gap events are thus compatible with the diffractive dissociation of a highly virtual photon by the proton. Such interactions are an excellent tool to study the structure of the Pomeron.[38,40,41]

Within the statistical uncertainty of the 1992 data, the large rapidity gap events exhibit the same Q^2 dependence as the standard DIS events. The important question whether their production is limited only to the small x region cannot be answered at this stage.

4 Limits on Exotic Particle Production

HERA is particularly well suited to searching for leptoquarks, which can be produced singly in the s-channel. The production depends only on the coupling of the leptoquark to the the incoming particles, the electron and a quark from the proton. We have searched in the 1992 data for leptoquarks in a sample of 1659 neutral current events and 2 charged current events. In the charged current events the leptoquark would decay to a quark and a neutrino. In the neutral current case leptoquark production would appear as a resonance in the x distribution at $x = M_{LQ}^2/s$. No evidence for a leptoquark is seen. We have set limits as a function of the coupling for various possible leptoquark states.[42] An example for a scalar leptoquark S_0[43] with $(e^- u)$ quantum numbers is shown in figure 18 for (a) right-handed coupling and (b) left-handed coupling.

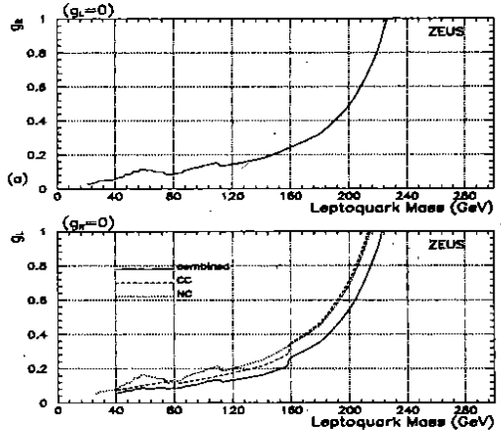

Figure 18: The 95% confidence level upper limits on the coupling of the scalar S_0 leptoquark versus mass for (a) left-handed coupling from the NC decay mode with branching ratio = 1; (b) right-handed coupling with branching ratio = 0.5 to each of the NC and CC modes.

At a reference (electroweak) coupling of $g = \sqrt{4\pi\alpha_{QED}} = 0.31$, the mass limits are 176 and 183 GeV for left and right-handed coupling, respectively. These are already higher than limits from CDF, where the production mechanism is a gluon coupling to leptoquark pairs.[44]

Leptogluons would also be produced in the s-channel by the coupling of the electron to a gluon in the proton. The coupling depends only on the gluon density in the proton and $(M_{LG}/\Lambda)^2$, where Λ is a scale parameter.[45] We exclude leptogluons of mass 100 GeV at Λ = 1.3 TeV.

The search for excited electron states (e^*) is a natural way to investigate the possibility of substructure. Various limits on the substructure scale have been derived mainly from e^+e^- experiments. Results from LEP experiments restrict $e^* \rightarrow e\gamma$ couplings for e^* masses up to the Z mass.[46] Complementary limits, due to virtual contributions and subject to model dependent assumptions, arise from data on $e^+e^- \rightarrow \gamma\gamma$, νe scattering, and electron gyromagnetic ratio measurements.[47] At HERA, excited electrons with masses up to the present kinematic limit of 296 GeV would be directly produced via the process ep$\rightarrow$e*X. This high centre of mass energy allows a search not only for the decay mode $e^* \rightarrow e\gamma$, but also for the decay modes $e^* \rightarrow \nu W$ and $e^* \rightarrow eZ$, which have not been investigated previously. We have searched for resonances in the $e\gamma$, νW ($W \rightarrow e\bar{\nu}, q\bar{q}$) and eZ ($Z \rightarrow e^+e^-, \nu\bar{\nu}, q\bar{q}$) final states. No evidence was found for an e^* state.[48] Exclusion limits for the coupling as a function of mass have been determined and are shown in figure 19.

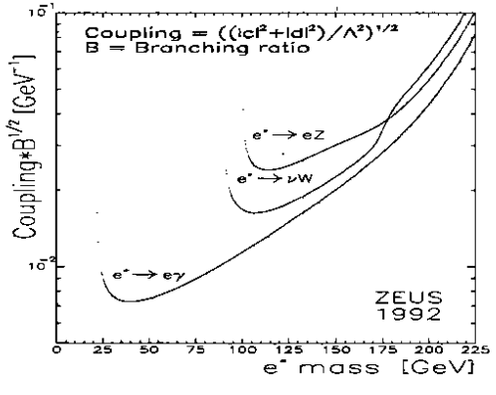

Figure 19: The 95% confidence level upper limits on the product of the coupling and the square root of the branching ratios for an e^* decaying to $e\gamma$, eZ and νW final states.

References

[1] A. Andresen et al., Nucl. Instr. and Meth. **A309** (101) 1991;
A. Bernstein et al., DESY 93-076 (1993), submitted to Nucl. Inst. and Meth.

[2] T. Sjöstrand, Z. Phys. **C42** (1989) 301;
H-U. Bengtsson and T. Sjöstrand, Comput. Phys. Commun. **46** (1987) 43.

[3] B.R. Webber, Ann. Rev. Nucl. Part. Sci. **36** (1986) 253;
G. Marchesini et al., Comput. Phys. Commun. **67** (1992) 465.

[4] N. N. Nikolaev and B. G. Zakharov, Z. Phys. **C53** (1992) 331 and LANDAU–16–93, to be published in Z. Phys. **C**.

[5] H1 Collab., T. Ahmed et al., Phys. Lett. **B299** (1993) 469.

[6] ZEUS Collab., M.Derrick et al., Phys. Lett. **B293** (1992) 465.

[7] Review of Particle Properties, Phys. Rev. **D45** (1992).

[8] H. Abramowicz, E.M. Levin, A. Levy and U. Maor, Phys. Lett. **B269** (1991) 465.

[9] A. Donnachie and P.V. Landshoff, Nucl. Phys. **B244** (1984) 322;
P.V. Landshoff, Nucl. Phys. B (Proc. Suppl.) **18C** (1990) 211.

[10] G.A. Schuler, Proc. of the Workshop on Physics at HERA, DESY (1992) 461;
A. Levy, ibid, 481.

[11] M. Drees and K. Grassie, Z. Phys. **C28** (1985) 451.

[12] G.A. Schuler, T.Sjöstrand, Phys. Lett. **B300** (1993) 169;
G.A. Schuler, T.Sjöstrand, CERN-TH.6796/93.

[13] M. Drees and F. Halzen, Phys. Rev. Lett. **61** (1988) 275;
M. Drees and R. M. Godbole, Phys. Rev. **D39** (1989) 169 and BU–TH–92/5.

[14] For a review see H. Abramowicz, K. Charchula, M. Krawczyk, A. Levy and U. Maor, Int. J. of Mod. Phys. **A8** (1993) 1005;
L. E. Gordon and J. K. Storrow, MC–TH–91–29.

[15] J. Huth et al., Proceedings of the 1990 DPF Summer study on HEP, Snowmass, Colorado, ed. E. L. Berger, World Scientific, Singapore 1992.

[16] ZEUS Collab., M. Derrick et al., Phys. Lett. **B297** (1992) 404.

[17] S. Bentvelsen, J.Engelen and P.Kooijman, Proc. of the Workshop on Physics at HERA, DESY (1992) 23.

[18] HERACLES 4.1: A.Kwiatkowski, H.Spiesberger and H.-J.Möhring, Proc. of Workshop on Physics at HERA, DESY, (1992) 1294;
A.Kwiatkowski, H.Spiesberger and H.-J.Möhring, Z. Phys. **C50** (1991) 165.

[19] B. Andersson et al., Z. Phys. **C43** (1989) 625.

[20] ARIADNE 3.1: L.Lönnblad, Comput. Phys. Commun. **71** (1992) 15.

[21] JETSET 6.3: T.Sjöstrand, Comput. Phys. Commun. **39** (1986) 347.

[22] A.D.Martin, R.G.Roberts and W.J.Stirling, Phys. Lett. **B306** (1993) 145.

[23] ZEUS Collab., M. Derrick et al., Phys. Lett. **B316** (1993) 412

[24] CTEQ collaboration: J. Botts et al., Phys. Lett. **304B** (1993) 159.

[25] M. Glück, E. Reya and A. Vogt, Phys. Lett. **306B** (1993) 391.

[26] H1 Collab., I. Abt et al., DESY 93-117, to be published in Nucl. Phys. **B**.

[27] ZEUS Collab., M.Derrick et al.,Z. Phys. **C59** (1993) 231.

[28] ZEUS Collab., M. Derrick et al, Phys. Lett. **B306** (1993) 158.

[29] ZEUS Collab., M. Derrick et al., Phys. Lett. **B315** (1993) 481.

[30] L. V. Gribov, E. M. Levin and M. G. Ryskin, Phys. Rep. 100 (1983) 1.

[31] E. L. Berger, J. C. Collins, D. E. Soper and G. Sterman, Nucl. Phys. **B286** (1987) 704.

[32] A. Donnachie and P.V. Landshoff, Nucl. Phys. **B311** (1989) 509 and Phys. Lett. **B285** (1992) 172.

[33] J. Bartels and G. Ingelman, Phys. Lett. **B235** (1990) 175.

[34] M. G. Ryskin, Sov. J. Nucl. Phys. **53** (1991) 668.

[35] G. Ingelman and K. Prytz, Phys. Lett. B281 (1992) 325 and Z. Phys. C58 (1993) 285.

[36] J. C. Collins, L. Frankfurt, M. Strikman, Phys. Lett. **B307** (1993) 161.

[37] E. Levin and M. Wüsthoff, DESY 92-166, FERMILAB-Pub-93/334.

[38] G. Ingelman and P. E. Schlein, Phys. Lett. **B152** (1985) 256.

[39] UA8 Collab., R. Bonino et al., Phys. Lett. **B211** (1988) 239;
A. Brandt et al., Phys. Lett. **B297** (1992) 417.

[40] A. Donnachie and P. V. Landshoff, Phys. Lett. **B191** (1987) 309.

[41] K. H. Streng, Proc. of the Workshop on Physics at HERA, DESY (1987) 365; CERN-TH.4949 (1988)

[42] ZEUS Collab., M. Derrick et al., Phys. Lett. **B306** (1993) 173.

[43] W. Buchmüller et al., Phys. Lett. **B191** (1987) 442;
B. Schrempp, Proc. of the Workshop on Physics at HERA, DESY (1992) 1034.

[44] CDF Collab., S. Moulding, Fermilab CONF-92-341-E (1992).

[45] J. Bijnens, Proc. of the Workshop on Physics at HERA, DESY (1987) 819;
K. H. Streng, Z. Phys. **C33** (1986) 247.

[46] OPAL Collab., M. Z. Akrawy et al.,Phys. Lett. **B257** (1991) 531;
DELPHI Collab., P. Abreu et al., Z. Phys. **C53** (1992) 41;
L3 Collab., O. Adriani et al., Phys. Lett. **B288** (1992) 404;
ALEPH Collab., D. Decamp et al., Phys. Rep. **216** (1992) 253.

[47] For a complete list of references, see.[48]

[48] ZEUS Collab., M. Derrick et al., Phys. Lett. **B316** (1993) 207.

Acknowledgements

The outstanding dedicated effort of our colleagues on ZEUS, the DESY technical staff and the ZEUS engineers and technicians, which made ZEUS a big success, is acknowledged. It is a pleasure to commend the HERA machine group for their achievement in commissioning and operating this complex new collider. Just at the time of submission of this paper, HERA has reached the goal of delivering an integrated luminosity of 1 pb^{-1} in 1993. The support of the DESY directorate is greatly appreciated.